Metallography, Microstructure, and Analysis (2019) 8:479–487
https://doi.org/10.1007/s13632-019-00556-x

TECHNICAL ARTICLE

Effect of Heat Treatments on the Mechanical and Electrochemical Corrosion Behavior of 38CrSi and AISI 4140 Steels

Muhammad Arslan Hafeez[1] · **Ameeq Farooq**[1]

Received: 9 May 2018 / Revised: 20 February 2019 / Accepted: 1 July 2019 / Published online: 10 July 2019

Abstract
The aim of this investigation was to compare the microstructural, mechanical and electrochemical corrosion characteristics of 38CrSi steel with widely used AISI 4140 steel under various heat treatment processes to widen its field of applications. Experimental steels 38CrSi and AISI 4140 were subjected to austenitizing at 900 °C for 30 min followed by annealing, quenching in oil and quenching followed by tempering at 400 °C for 120 min. Microstructure of 38CrSi and AISI 4140 steels was characterized by light optical and scanning electron microscopy. Tensile, Charpy impact toughness and Rockwell hardness testing techniques were used to evaluate the mechanical properties. Electrochemical corrosion behavior was evaluated by a Tafel scan in tape water. Results show that microstructure of both steels comprised of ferrite and pearlite after annealing, packets and blocks of lath martensite with retained austenite after quenching and tempered lath martensite with retained austenite after quenching, and tempering with varying grain size distribution and volume fractions of different phases. Hardness and tensile properties of both steels varied in quite identical manner, while impact toughness of both steels varied in inverse manner. 38CrSi steel was found to be brittle, while AISI 4140 steel exhibited excellent properties under all heat treatment processes. In 38CrSi, the corrosion rate decreases as compared to the as-received sample from 0.515 to 0.486 mpy in quenching and tempering heat treatment, while in AISI 4140 steel the corrosion rate decreases during quenching from 0.620 to 0.472 mpy.

Keywords Retained austenite · Tafel scan · Martensite · Tempering

Introduction

Heat treatments and manufacturing processes impact the materials behavior during specific applications. Due to this significant importance, many studies are carried out in the last few years [1, 2]. Some researchers investigated the influence of annealing processes on characteristics of steels such as SCM435 steel [3], medium carbon steel [4], 30% Cr super ferritic stainless steel [5], Fe–Si steel [6], Fe–25Cr–20Ni steel [7] and TRIP steel [8, 9], while some focused on characteristics of steels like 30CrMnSiNi2A steel [10], low-carbon martensitic steels [11], 718H steel [12], 3Mn–Si–Ni martensitic steel [13], Cr14 ultra-high-strength steel [14], 2.25Cr–1Mo–0.25V steel [15], medium carbon bainitic steel [16], medium-Mn TRIP steels [17], HSLA steel [18], reactor pressure vessel steel [19], 300M steel [20], Aermet 100 steel [21], P92 steel [22], mooring chain steel [23], X12CrMoWVNbN10-1-1 steel [24], non-quenched bainitic steel [25] and AISI 4140 steel [1, 2, 26] under quenched and tempered conditions. 38CrSi steel is a medium alloyed experimental steel used in manufacturing of general machinery components due to its high hardness [27]. There is great need of investigating its characteristics under various heat treatment processes in comparison to some other widely used materials such as AISI 4140 steel which is used in manufacturing of gears, bolts, couplings, spindles, tool holders, sprockets, oil industry drill collars and tools joints [26]. Xiong et al. [6] found that stress relief annealing significantly lowered the dislocation densities and the low-angle grain boundary percentages, refined grain sizes and improved the hysteresis loops of Fe–Si steel. Xiong et al. [7] reported that best amalgamation of mechanical properties of cryo-rolled Fe–25Cr–20Ni steel can be achieved by annealing at temperature greater than 800 °C for 10 min. Xu

✉ Ameeq Farooq
ameeq.farooq@gmail.com

[1] Corrosion Control Research Cell, Department of Metallurgy and Materials Engineering, CEET, University of the Punjab, Lahore 54590, Pakistan

et al. [8] reported that inter-critical annealing significantly improves the tensile strength and slightly reduced elongation than one step annealing and transformed lathe austenite into block like austenite in hot rolled medium manganese TRIP steel containing δ-ferrite. Ma et al. [5] reported that an increase in annealing temperature improves the strength, hardness and reduces elongation of 30% Cr super ferrite stainless steel. Similarly, Cheng et al. [3] also showed that an increase in annealing temperature improves the spheroidization ratio, mechanical properties and formability of SCM435 steel. On the other hand, Hafeez et al. [10] reported that optimum amalgamation of characteristics of 30CrMnSiNi2A steel achieved at 350 °C for 3 h of tempering temperature. Martensite transformed into ε-carbide, cementite, coarsened and spheroidized cementite, and ferrite and austenite with increasing tempering temperature [9]. Wang et al. [9] showed that quenching at 780 °C for 15 min gives the best combination of tensile properties for hot rolled TRIP sheet steel [13]. Zhang et al. [14] reported that an increase in tempering temperature causes increasingly segregated carbides, an increase in tensile strength and decreases in yield strength, elongation, impact toughness and fracture toughness of Cr14 ultra-high-strength steel. Jiang et al. [15] found that 0.5 h tempering improved, while 0.5–128 h tempering reduced the strength and ductile to brittle transition temperature of normalized samples greater than oil quenched samples of 2.25Cr–1Mo–0.25 V steel. Kang et al. [16] found that medium carbon bainitic steel gives the most suitable combination of strength and toughness with specific plasticity level at a 340 °C of tempering temperature. Li et al. [17] reported that increasing annealing time lead to carbon and manganese enrichment of austenite, deterioration of the transformation-induced plasticity (TRIP) effect and reduction in dislocation density and work-hardening rates. The quenching and tempering process caused enrichment of elements, stability of the TRIP effect and the best combination of mechanical properties and high dislocation density in austenite. Lu et al. [28] reported that quenched 13% Cr martensitic stainless steel exhibited a much higher pitting potential than tempered steel. A gradual reduction in pitting potential was observed with the increase in tempering temperature. At 500 °C, tempering significantly reduced corrosion resistance of the steel. Before undergoing practical use, almost all the steels subjected to some heat treatment process to achieve suitable amalgamation of mechanical properties. Since the working temperature can vary from a low to sufficiently high value, which may cause alteration in microstructure along with composition in the adjacent region. This alteration can result in modification of mechanical properties, pitting sensitization and reduction in corrosion resistance [28]. Therefore, there is a great need for investigating the effect of heat treatment processes on mechanical and electrochemical corrosion properties of steels. In the present work, the effect of heat treatment on microstructure, mechanical properties like tensile properties, impact toughness and hardness of 38CrSi and AISI 4140 steels was investigated. Tafel scanning was also carried out to analyze the variation in polarization and corrosion behavior under various heat treatments.

Experimental Work

Material

38CrSi and AISI 4140 steels were obtained in the form of 30 mm diameter rods produced by melting in a vacuum induction furnace, casting in a continuous casting machine and rolling into final shape. The chemical composition of these steels is given in Table 1. Wet sectioning was carried out to cut 152.4-mm-long pieces for subsequent heat treatment processes.

Heat Treatment

The samples of 38CrSi and AISI 4140 were austenitized at 900 °C for 30 min. Three samples were annealed by furnace cooling, three were quenched by immersing in Quench 310 oil, and three were quenched in the same manner and tempered at 400 °C for 120 min. The schematic heat treatment cycles are shown in Fig. 1. After heat treatment, all the samples were degreased in an alkaline cleaning solution of 10% NaOH solution for 10 min at 60 °C.

Microstructure Analysis

For microstructure analysis, samples were cut by wet sectioning into 10 × 10 × 10 mm samples then ground manually on P60, P120, P220, P400, P600, P800 and P1000 grades of silicon carbide (SiC) papers and polished on automatic polisher (*Ecomet 250 Grinder Polisher*, *USA*). For rough polishing, a nylon cloth with diamond pastes of 3 and 6 microns was used, whereas for fine polishing, velvet cloth with diamond pastes 0.25 and 1 microns was used. Samples were then etched in freshly prepared 2% nital for 15 s,

Table 1 Chemical composition of steels (wt.%)

Material	C	Si	Mn	Cr	Mo	S	P
38CrSi	0.40	1.01	0.57	1.36	0.07	0.02	0.01
AISI 4140	0.40	0.22	0.90	1.00	0.20	0.03	0.02

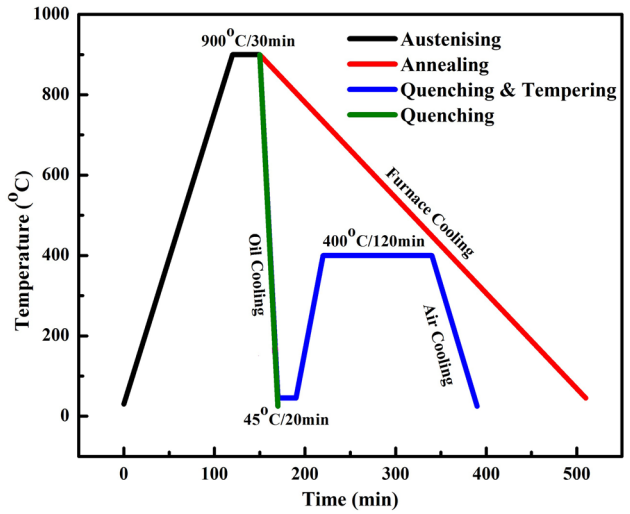

Fig. 1 Heat treatment cycles applied on 38CrSi and AISI 4140

rinsed in ethanol and dried by a hot air dryer. Microstructure evaluation was performed on light optical microscope (*Leica Model DM 15000M, Germany*) and scanning electron microscope (*Hitachi SU-8000 Japan*).

Mechanical Testing

Hardness testing was performed on polished samples of dimension 10 × 10 × 10 mm by a Rockwell hardness tester (*Insize ISH-R150, China*) under diamond cone indenter with load of 1471 N for 10 s on Rockwell hardness scale 'C.' The hardness value was calculated by taking the average of three readings. For tensile testing, rods were machined into samples of gauge length 50.8 mm, gauge diameter 12.7 mm, fillet radius 9.525 mm and reduced section length 57.15 mm according to the ASTM E8 standard. Testing was performed on a computer control universal testing machine (*Kelson's, India*). For impact testing, samples of length 75 mm, square cross section of side length 10 mm, notch depth 2 mm, notch angle 45° and notch to edge distance 28 mm were designed according to the ASTM E23 standard. Impact testing was performed on a Charpy impact tester (*Avery Denison, USA*) under a load of 300 J.

Electrochemical Corrosion Testing

The working electrode was connected with copper wire for electrical connection by soldering and cold mounted in polyester resin by exposing 1 cm^2 surface area. Before electrochemical corrosion testing, the working electrodes were ground to P220, P600, P800 and P1000. Tape water (pH 7.55, conductivity 239 µS cm^{-1}, TDS 155 mg L^{-1}, hardness 90 mg L^{-1}, chloride 7 mg L^{-1}, bicarbonates 110 mg L^{-1}, sulfates 21 mg L^{-1}) was used as an electrolyte for electrochemical corrosion testing at room temperature. Saturated calomel was used as a reference, and platinum wire was used as the counter electrode in three electrode cell system coupled with an Autolab potentiostat (*Metrohm PG30, Netherlands*). Tafel scanning was used to investigate the polarization behavior and corrosion kinetics in tape water.

Results and Discussion

Microstructure

Micrographs of 38CrSi and AISI 4140 steels captured by light optical and scanning electron microscopes after various heat treatment processes are illustrated in Figs. 2, 3, 4 and 5. Microstructures of as-received 38CrSi and AISI 4140 steels comprised of pearlite randomly distributed in the matrix of ferrite with a difference of grain size. 38CrSi steel contains larger grains than AISI 4140 steel as presented in Fig. 2a and b. The presence of these phases was validated by high-magnification SEM micrographs Fig. 3a and b. As a result of austenitizing, microstructure of both steels fully transformed into austenite. The annealing process produced uniformly distributed pearlite in the matrix of ferrite with pearlite in larger fractions as previously reported by Lu et al. [4]. At this stage, phases become clear and easy to identify Figs. 2c, d and 3c, d.

After quenching of both steels, austenite partially transformed into packets and blocks of lath martensite along with fractions of retained austenite in accordance with the work of Zhang et al. [14] as presented in Fig. 4a and b and high-magnification SEM micrographs Fig. 5a and b. Tempering is performed on steel after quenching to achieve stable tempered martensite and retained austenite along with precipitation of secondary phases causes improved material properties [14]. When the quenched samples are tempered at 400 °C, excess carbon in the supersaturated lath martensite diffuses out, precipitation of secondary phases like epsilon carbides or cementite occurred, and stable tempered martensite achieved in accordance with [2, 16, 18, 21] as presented in Figs. 4c, d and 5c, d.

Mechanical Properties

Tensile Properties

Variation in tensile properties of 38CrSi and AISI 4140 with various heat treatment processes is plotted in Table 2. Tensile properties of both steels are observed to be highly dependent on heat treatments and resulting microstructures. In the as-received (AR) condition, 38CrSi steel exhibited better tensile strength (944 MPa), significantly higher

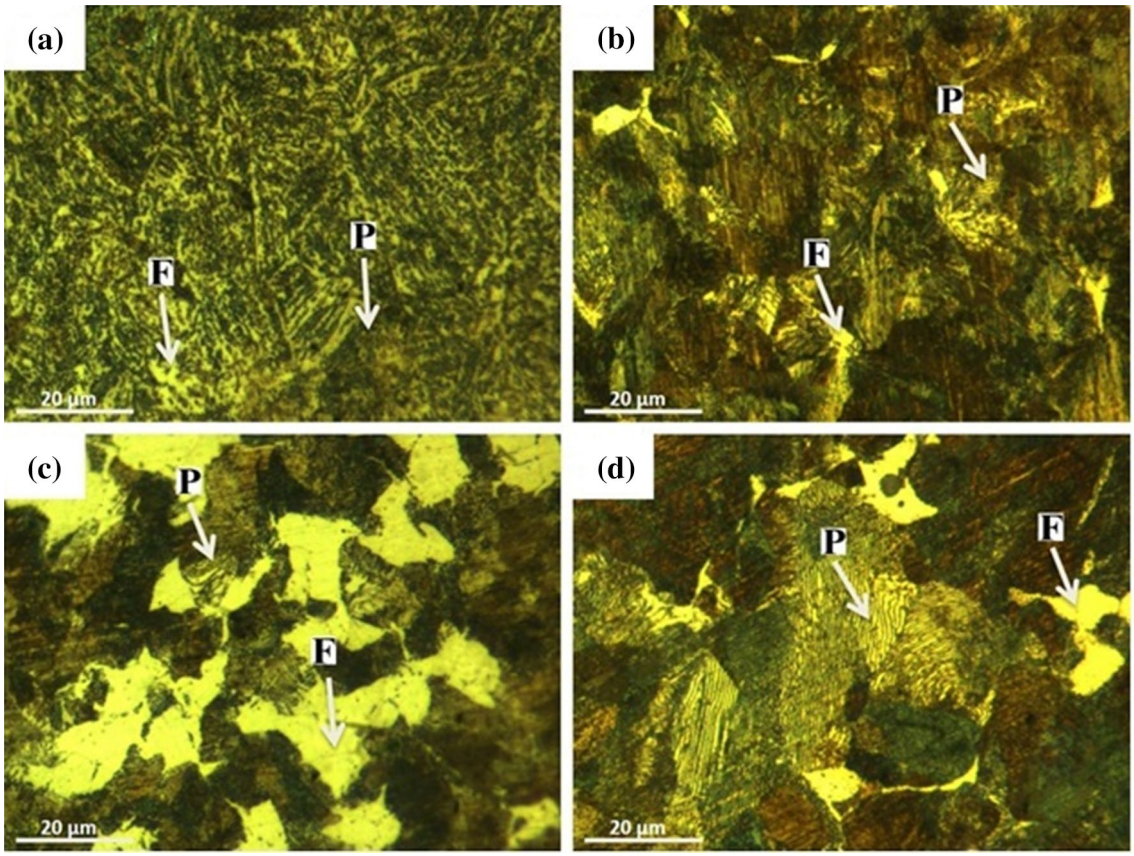

Fig. 2 Optical micrographs of AISI 4140 and 38CrSi (**a**, **b**) as received, (**c**, **d**) annealed at × 1000 magnification

elongation (17%) and reduction in area (54%) than AISI 4140. 38CrSi steel which is attributed to the larger fractions of ferrite with pearlite in finer grain size than AISI 4140. Tensile strength of both steels slightly reduced after annealing (A) due to the uniform distribution and coarsening of ferrite and pearlite grains. Elongation and reduction in area of annealed AISI 4140 (20 and 54%) are significantly improved because it contains ferrite in greater fractions, while in case of 38CrSi it was reduced which is due to the greater fractions of pearlite. When these steels are subjected to oil quenching (Q), they exhibit improved strength, and significantly reduced elongation and reduction in area due to the formation of packets and blocks of lath martensite which is brittle in nature. Tempering of AISI 4140 steel at 400 °C results in significant improvement in tensile strength (1583 MPa), elongation (7%) and reduction in area (45%) compared to quenched steel which is due to the diffusion of excess carbon from martensite into austenite and secondary phase particles, and interaction of secondary phase carbides with dislocation as previously described by Kang et al. [16]. The behavior of 38CrSi steel after quenching and tempering (QT) was similar to AISI 4140 for tensile strength as it improved to (1703 MPa) but was quite different in case of elongation and reduction in area showing slight improvement to 1.47 and 4.55%, respectively. This unusual behavior might be due to the higher percentage of chromium and silicon which caused brittleness of material.

Impact Toughness

Impact toughness reflects the resistance of metal materials to external shock loads. Steel with a poor toughness has a low impact toughness value [14]. The behavior of 38CrSi steel under impact loads is quite different from AISI 4140 steel as shown in Fig. 6. In the as-received (AR) condition, 38CrSi and AISI 4140 steels show a similar impact toughness of 14 and 18 J, respectively. After annealing (A) experimental steels showed the inverse behavior as 38CrSi became more brittle showing reduced impact toughness of 10 J while AISI 4140 became fully ductile showing maximum impact toughness of 40 J which is due to the presence of greater percentage of Cr with sufficient amount of Mn in 38CrSi which enhance the fractions of pearlite and make this steel more brittle, while in AISI 4140 formation of sufficient fractions of ferrite makes this steel more ductile. During quenching (Q) which always caused brittleness in steels, impact toughness reduced for 38CrSi and AISI 4140 steels after quenching (Q) as 8 and 21 J, respectively. The

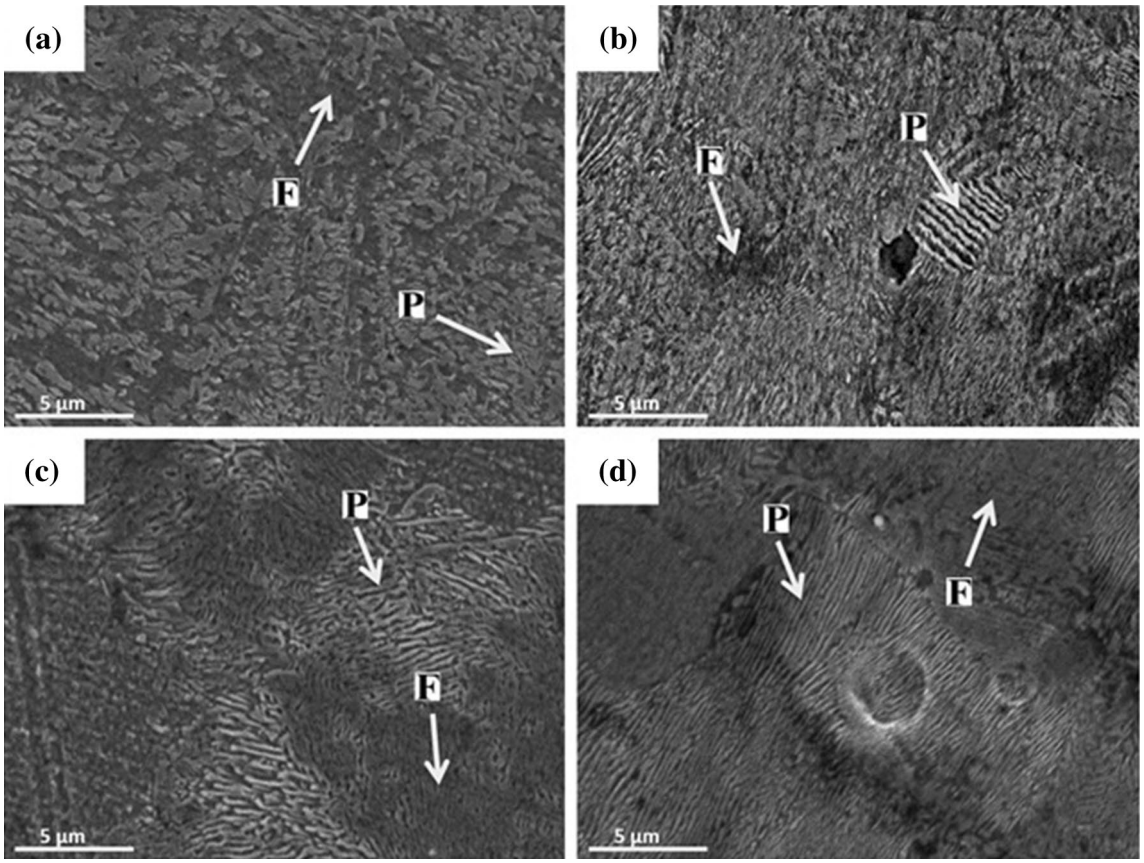

Fig. 3 SEM images of AISI 4140 and 38CrSi (**a**, **b**) as received, (**c**, **d**) annealed

38CrSi steel showed extreme brittle behavior in quenched form which is attributed to the formation of supersaturated lath martensite in excess fractions. On the other hand, AISI 4140 steel showed a moderate level of impact toughness after quenching (Q) due to lower fractions of lath martensite than 38CrSi steel. Quenching and tempering process (QT) reduced the brittleness and improved the impact toughness for both steels by transferring the excess carbon from lath martensite to austenite or secondary phases.

Hardness

The Rockwell hardness results of 38CrSi and AISI 4140 steels after annealing, quenching and quenching-tempering processes are shown in Fig. 7. It can be observed that in as-received (AR) samples of both steels possess moderate hardness values, but 38CrSi steel (22 HRC) has lower hardness value than AISI 4140 steel (28 HRC) which is attributed to the presence of greater percentage of silicon in 38CrSi steel which suppress the formation of carbides results in larger fractions of ferrite and lower fractions of pearlite with larger grain size, while in AISI 4140 due to presence of Mo and Mn in greater percentage which promotes hardness in the as-received form. After annealing (A), hardness values reduced for both steels, but 38CrSi steel exhibited less reduction in hardness than AISI 4140. It is due to the fact that the larger volume fractions of pearlite formed due to higher percentage of chromium and silicon in 38CrSi, while in AISI 4140 steel the formation of sufficient fractions of ferrite caused significant reduction in hardness. After quenching (Q), a drastic increase in hardness was observed which is caused by the formation of packets and blocks of lath martensite. 38CrSi (53 HRC) shows greater hardness in the quenched condition than AISI 4140 (49 HRC) due to the presence of a greater percentage of Cr and Si with a sufficient amount of Mn which promotes the formation of martensite Fig. 7. When the steels were quenched and tempered (QT) at 400 °C, hardness of both steels reduced due to the decomposition of martensite, and retained austenite, and formation of secondary phase carbides [2, 16, 18, 21].

Electrochemical Corrosion Properties

Tafel scans of 38CrSi and AISI 4140 after various heat treatments in tape water are shown in Fig. 8. The polarization behavior was evaluated in the potential range of − 0.25 to

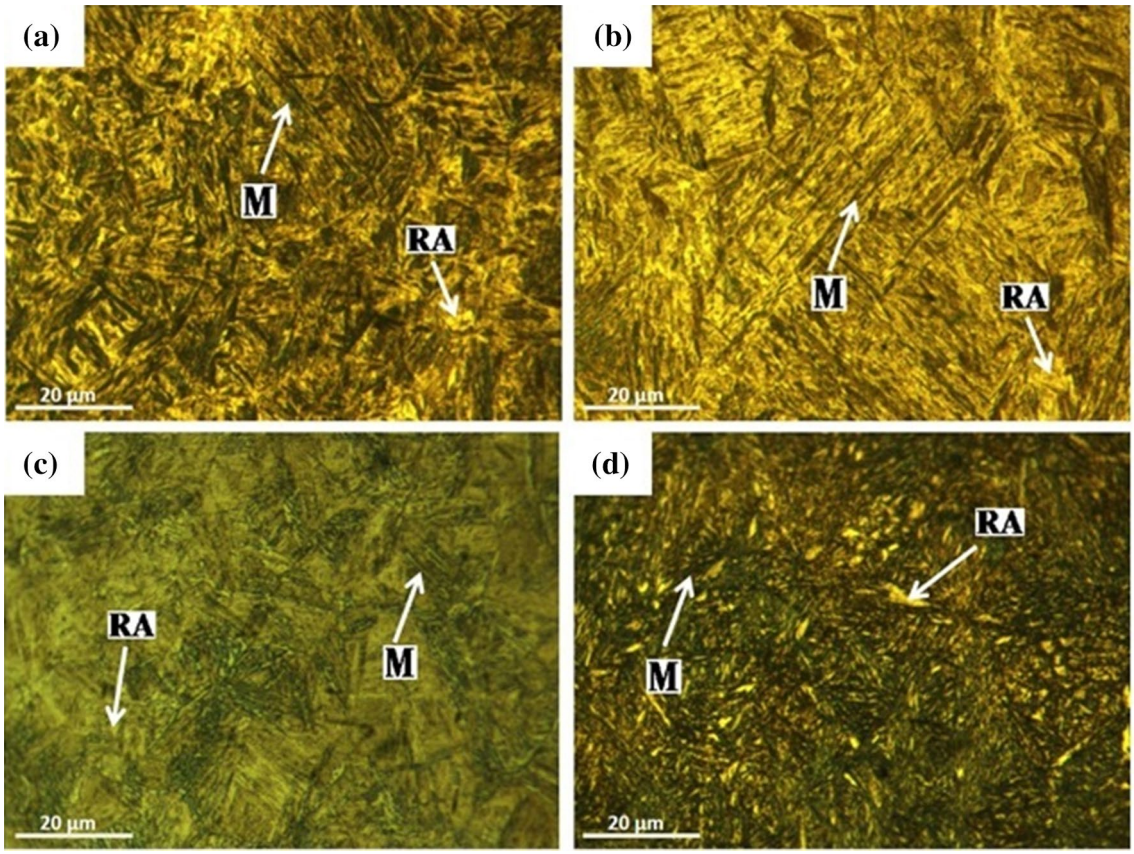

Fig. 4 Optical micrographs of AISI 4140 and 38CrSi (**a**, **b**) quenched, (**c**, **d**) quenched and tempered at × 1000 magnification

0.25 V with respect to open circuit potential with a scan rate of 1 mV/s. The kinetic parameters were calculated by a Tafel extrapolation method using *NOVA 2.1* software as shown in Table 3. According to the Butler–Volmer relation [29]:

$$i_{\text{net}} = i_o \left\{ \exp\left(\beta_a \frac{nF}{RT}\eta_a\right) | - \exp\left[-\left(1-\beta_c\right)\frac{nF}{RT}\eta_c\right] \right\}$$

where 'β_a' and 'β_c' are the anodic and cathodic Tafel constants. 'η_a' and 'η_c' represent the anodic and cathodic polarization of the metal surfaces during Tafel extrapolation.

The electrochemical corrosion behavior of both 38CrSi and AISI 4140 changes with different heat treatment. I_{corr} and E_{corr} are the corrosion current density and potential, respectively. The anodic and cathodic polarization slope of the Tafel scan is represented by β_a and β_c, respectively. In the case of as-received (AR) condition, 38CrSi has a β_a value of 83 mV decade^{-1} greater as compared to 64 mV decade^{-1} of AISI 4140 which shows that in the as-received condition the 38CrSi has less metal dissolution as compared to AISI 4140. The corrosion current density of 38CrSi which is 1.129 µA cm^{-2} results in a lower corrosion rate of 0.515 mpy as compared to AISI 4140 with 1.357 µA cm^{-2} and 0.620 mpy. The higher current density resulting in a higher corrosion rate is according to Butler–Volmer relation [29]. 38CrSi microstructure shows a larger grain size than AISI 4140 in the as-received condition and a random distribution of pearlite in the matrix of ferrite so its corrosion rate decreases due to fewer grain boundaries. As both the steels were annealed in the same conditions then due to furnace cooling the grain size increases, but amount of pearlite in the matrix of ferrite also increases as shown in Fig. 2c and d. The ferrite content in the microstructures of the steel will increase the corrosion rate [30]. In the case of 38CrSi steel after annealing (A), the increase in the corrosion rate to 0.678 mpy from 0.515 mpy in the as-received condition is due to an increase in the ferrite content, while for AISI 4140 after annealing (A) the grain size increase results in a decrease of 0.523 mpy from 0.620 mpy compared to the as-received condition. When both steels were quenched in oil, due to fast cooling rate the martensite and austenite phases are formed as shown in Fig. 3a and b which reduces the corrosion rate as compared to the as-received samples [30]. After quenching, in 38CrSi steel the corrosion rate decreases to 0.495 mpy compared to 0.515 mpy in the as-received condition which means the heat treatment will affect the electrochemical corrosion behavior significantly. But in AISI 4140 steel the corrosion

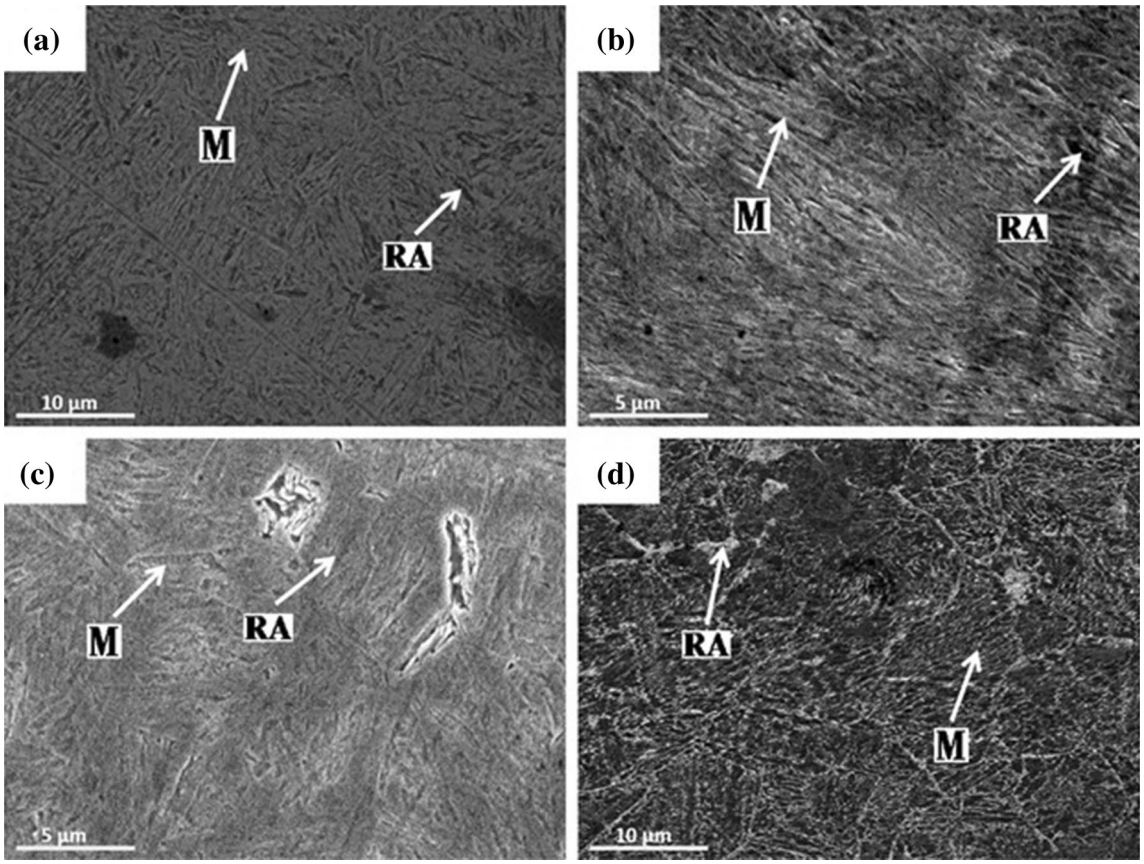

Fig. 5 SEM images of AISI 4140 and 38CrSi (**a**, **b**) quenched, (**c**, **d**) quenched and tempered

Table 2 Tensile properties of 38CrSi and AISI 4140

Samples ID	Tensile strength (MPa)	Elongation (%)	Reduction in area (%)
38CrSi			
AR	943.609	16.86	54.58
A	854.947	14.49	34.58
Q	1030.610	0.64	1.58
QT	1703.223	1.47	4.55
AISI 4140			
AR	782.650	3.76	3.25
A	760.976	19.72	54.33
Q	1035.631	0.44	1.44
QT	1582.654	7.05	45.13

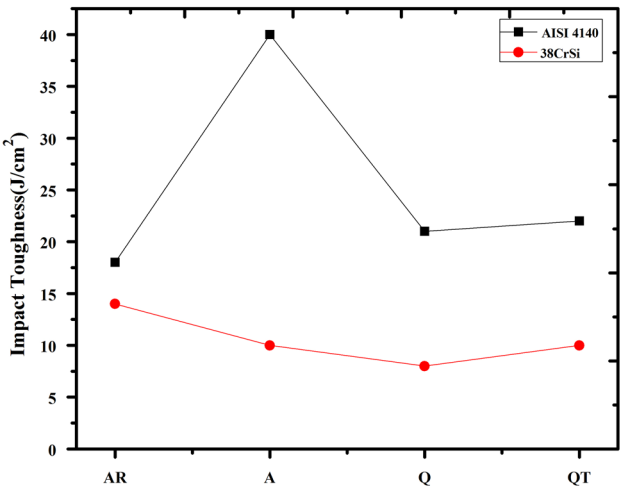

Fig. 6 Impact toughness profile of 38CrSi and AISI 4140 under various heat treatments

rate significantly decreases after quenching from 0.620 to 0.472 mpy due to the formation of lath martensite and austenite phases. The presence of lath martensite increases the hardness, so in many applications the high hardness increases the deterioration of steel component. So quenching and tempering was performed to overcome this problem. After quenching and tempering, the corrosion rate in 38CrSi further decreases to 0.486 mpy, while in AISI 4140 it increases to 0.778 mpy. So, the quenching and tempering has adverse effect on the electrochemical corrosion behavior of AISI 4140.

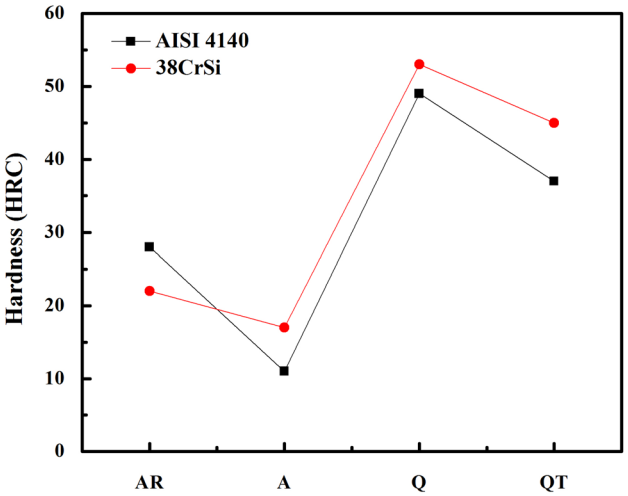

Fig. 7 Hardness profile of AISI 4140 and 38CrSi after different heat treatments

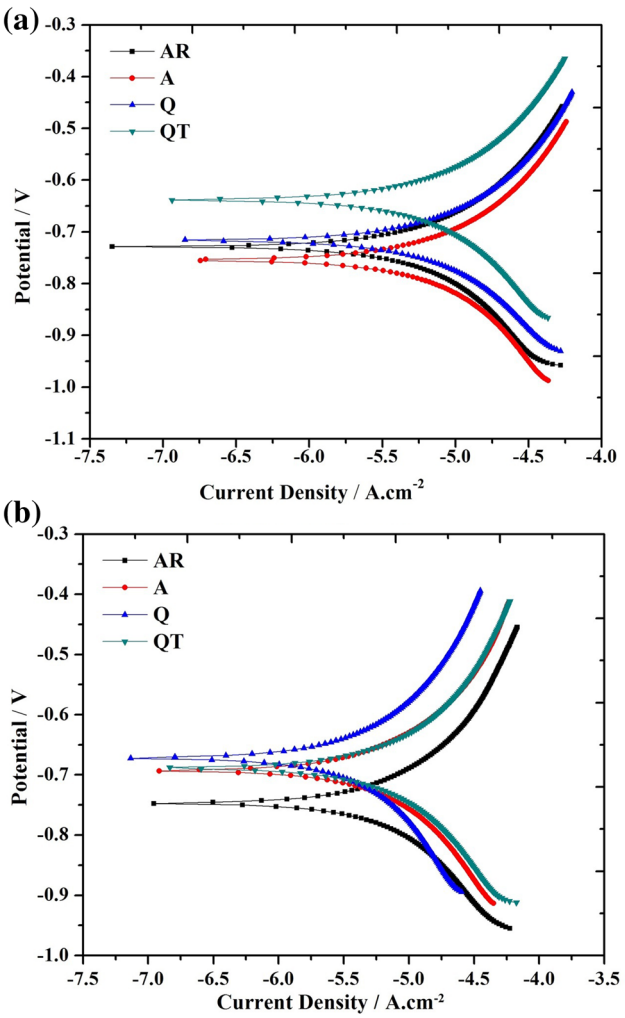

Fig. 8 Tafel Scan of (**a**) 38CrSi and (**b**) AISI 4140

Table 3 Kinetic parameters of heat-treated 38CrSi and AISI 4140

Samples	β_a (mV/decades)	β_c (mV/decades)	I_{corr} (μA cm^{-2})	E_{corr} (mV)	Corrosion rate (mpy)
38CrSi					
AR	83	105	1.129	−734	0.515
A	100	119	1.483	−760	0.678
Q	71	84	1.084	−719	0.495
QT	68	99	1.064	−645	0.486
AISI 4140					
AR	64	119	1.357	−758	0.620
A	80	101	1.146	−697	0.523
Q	111	137	1.035	−679	0.472
QT	106	128	1.701	−693	0.778

Conclusion

Microstructural, mechanical and electrochemical corrosion properties of 38CrSi steel were systematically compared with AISI 4140 steel as a function of various heat treatment processes. Significant variations in characteristics were observed for all heat treatment processes. The following conclusions can be extracted from this investigation:

1. After an annealing process, 38CrSi possessed larger fractions of pearlite and smaller fractions of ferrite than AISI 4140; therefore, it exhibited slightly greater hardness, tensile strength, corrosion resistance and sufficiently lower elongation, reduction in area and impact toughness. The behavior of 38CrSi was observed to be brittle after annealing.
2. After a quenching process, slightly larger fractions of packets and blocks of lath martensite with smaller fractions of retained austenite produced in 38CrSi are compared to AISI 4140 steel and showed slightly greater hardness, almost equal tensile strength, elongation and reduction in area but significantly lowered impact toughness
3. After a quenching and tempering process, diffusion of carbon from lath martensite into austenite and secondary phase particles results in improved strength, impact toughness and reduced elongation, reduction in area and Vickers hardness in 38CrSi and AISI 4140 steels as compared to the as-received condition.
4. 38CrSi steel is more brittle than AISI 4140 steel on the basis of impact toughness behavior under all heat treatments.
5. Quenching and tempering heat treatment technique reduced the corrosion rate of 38CrSi compared to as-received sample.

References

1. A.D. da Silva, T.A. Pedrosa, J.L. Gonzalez Mendez, X. Jiang, P.R. Cetlin, T. Altan, Distortion in quenching an AISI 4140 C-ring predictions and experiments. Mater. Des. **42**, 55–61 (2012)
2. M.H. KhaniSanij, S.S. GhasemiBanadkouki, A.R. Mashreghi, M. Moshrefifar, The effect of single and double quenching and tempering heat treatments on the microstructure and mechanical properties of AISI 4140 steel. Mater. Des. **42**, 339–346 (2012)
3. J.I. Cheng, W. Lei, M.Y. Zhu, Effect of subcritical annealing temperature on microstructure and mechanical properties of SCM435 steel. J. Iron Steel Res. Int. **22**, 1031–1036 (2015)
4. Z. Lü, H.F. Zhang, Q. Meng, Z.H. Wang, W.T. Fu, Effect of cyclic annealing on microstructure and mechanical properties of medium carbon steel. J. Iron Steel. Res. Int. **23**, 145–150 (2016)
5. L. Ma, S. Hu, J. Shen, J. Han, Effects of annealing temperature on microstructure, mechanical properties and corrosion resistance of 30% Cr super ferritic stainless steel. Mater. Lett. **184**, 204–207 (2016)
6. X. Xiong, S. Hu, N. Dang, K. Hu, Effect of stress-relief annealing on microstructure, texture and hysteresis curve of mechanically cut non-oriented Fe-Si steel. Mater. Charact. **132**, 239–247 (2017)
7. Y. Xiong, T. He, H. Li, Y. Lu, F. Ren, A.A. Volinsky, Annealing effects on microstructure and mechanical properties of cryorolled Fe–25Cr–20Ni steel. Mater. Sci. Eng. A **703**, 68–75 (2017)
8. Y. Xu, Z.P. Hu, Y. Zou, X.D. Tan, D.T. Han, S.Q. Chen, D.G. Ma, R.D.K. Misra, Effect of two-step intercritical annealing on microstructure and mechanical properties of hot rolled medium manganese TRIP steel containing δ- ferrite. Mater. Sci. Eng. A **688**, 40–55 (2017)
9. H.S. Wang, J. Kang, W.X. Dou, Y.X. Zhang, G. Yuan, G.M. Cao, R.D.K. Misra, G.D. Wang, Microstructure and mechanical properties of hot-rolled and heat-treated TRIP steel with direct quenching process. Mater. Sci. Eng. A. **702**, 350–359 (2017)
10. M.A. Hafeez, A. Farooq, Microstructural, mechanical and tribological investigation of 30CrMnSiNi2A ultra-high strength steel under various tempering temperatures. Mater. Res. Express **5**, 016505 (2018)
11. L.R.C. Malheiros, E.A.P. Rodriguez, A. Arlazarov, Mechanical behavior of tempered martensite: characterization and modeling. Mater. Sci. Eng. A **706**, 38–47 (2017)
12. H. Liu, P. Fu, H. Liu, C. Sun, X. Ma, D. Li, Microstructure evolution and mechanical properties in 718H pre-hardened mold steel during tempering. Mater. Sci. Eng. A **709**, 181–192 (2018)
13. Y.J. Zhao, X.P. Ren, Z.L. Hu, Z.P. Xiong, J.M. Zeng, B.Y. Hou, Effect of tempering on microstructure and mechanical properties of 3Mn–Si–Ni martensitic steel. Mater. Sci. Eng. A **711**, 397–404 (2018)
14. Y. Zhang, D. Zhan, X. Qi, Z. Jiang, H. Zhang, Microstructure and mechanical properties of Cr14 ultra-high-strength steel at different tempering temperatures around 773 K. Mater. Sci. Eng. A **698**, 152–161 (2017)
15. Z. Jiang, P. Wang, D. Li, Y. Li, The evolutions of microstructure and mechanical properties of 2.25Cr–1Mo–0.25V steel with different initial microstructures during tempering. Mater. Sci. Eng. A. **699**, 165–175 (2017)
16. J. Kang, F.C. Zhang, X.W. Yang, B. Lv, K.M. Wu, Effect of tempering on the microstructure and mechanical properties of a medium carbon bainitic steel. Mater. Sci. Eng. A **686**, 150–159 (2017)
17. Z.C. Li, H. Ding, R.D.K. Misra, Z.H. Cai, Microstructure mechanical property relationship and austenite stability in medium-Mn TRIP steels: the effect of austenite-reverted transformation and quenching-tempering treatments. Mater. Sci. Eng. A **682**, 211–219 (2017)
18. Y. Liu, L. Shi, C. Liu, L. Yu, Z. Yan, H. Li, Effect of step quenching on microstructures and mechanical properties of HSLA steel. Mater. Sci. Eng. A **675**, 371–378 (2016)
19. C.W. Li, L.Z. Han, X.M. Luo, Q.D. Liu, J.F. Gu, Effect of tempering temperature on the microstructure and mechanical properties of a reactor pressure vessel steel. J. Nucl. Mater. **477**, 246–256 (2016)
20. F. Liu, X. Lin, M. Song, H. Yang, K. Song, P. Guo, W. Huang, Effect of tempering temperature on microstructure and mechanical properties of laser solid formed 300 M steel. J. Alloys Compd. **689**, 225–232 (2016)
21. X. Shi, W. Zeng, Q. Zhao, W. Peng, C. Kang, Study on the microstructure and mechanical properties of Aermet 100 steel at the tempering temperature around 482 °C. J. Alloys Compd. **679**, 184–190 (2016)
22. D.R. Barbadikar, G.S. Deshmukh, L. Maddi, K. Laha, P. Parameswaran, A.R. Ballal, D.R. Peshwe, R.K. Paretkar, M. Nandagopal, M.D. Mathew, Effect of normalizing and tempering temperatures on microstructure and mechanical properties of P92 steel. Int. J. Press. Vessel. Pip. **132–133**, 97–105 (2015)
23. X.Y. Cheng, H.X. Zhang, H. Li, H.P. Shen, Effect of tempering temperature on the microstructure and mechanical properties in mooring chain steel. Mater. Sci. Eng. A **636**, 164–171 (2015)
24. X.G. Tao, L.Z. Han, J.F. Gu, Effect of tempering on microstructure evolution and mechanical properties of X12CrMoWVNbN10-1-1 steel. Mater. Sci. Eng. A **618**, 189–204 (2014)
25. Y. Luo, J. Peng, H. Wang, X. Wu, Effect of tempering on microstructure and mechanical properties of a non-quenched bainitic steel. Mater. Sci. Eng. A **527**, 3433–3437 (2010)
26. A.H. Meysami, R. Ghasemzadeh, S.H. Seyedein, M.R. Aboutalebi, An investigation on the microstructure and mechanical properties of direct-quenched and tempered AISI 4140 steel. Mater. Des. **31**, 1570–1575 (2010)
27. J.W. He, X.M. Wang, S.N. Ma, C.Q. Li, X.Q. Feng, Characterization and tribological properties of nanocrystalline surface layer of 38CrSi alloyed steel induced by SFPB. Rev. Adv. Mater. Sci. **33**, 19–23 (2013)
28. S.Y. Lu, K.F. Yao, Y.B. Chen, M.H. Wang, X. Liu, X. Ge, The effect of tempering temperature on the microstructure and electrochemical properties of a 13 wt.% Cr-type martensitic stainless steel. Electrochim. Acta **165**, 45–55 (2015)
29. P.R. Roberge, *Handbook of Corrosion Engineering* (McGraw-Hill, New York, 2000)
30. R.W. Revie, H.H. Uhlig, *Corrosion and Corrosion Control*, 4th edn. (Wiley, New York, 2008)